

Singularity Avoidance with Application to Online Trajectory Optimization for Serial Manipulators

F. Beck^{*,1}, M.N. Vu^{*,1}, C. Hartl-Nesic^{*}, A. Kugi^{*,**}

^{*} Automation and Control Institute (ACIN), TU Wien, Vienna, Austria (e-mail: {beck, vu, hartl, kugi}@acin.tuwien.ac.at).

^{**} Center for Vision, Automation and Control, AIT Austrian Institute of Technology, Vienna, Austria (e-mail: {andreas.kugi}@ait.ac.at)

Abstract: This work proposes a novel singularity avoidance approach for real-time trajectory optimization based on known singular configurations. The focus of this work lies on analyzing kinematically singular configurations for three robots with different kinematic structures, i.e., the COMAU Racer 7-1.4, the KUKA LBR iiwa R820, and the FRANKA EMIKA Panda, and exploiting these configurations in form of tailored potential functions for singularity avoidance. Monte Carlo simulations of the proposed method and the commonly used manipulability maximization approach are performed for comparison. The numerical results show that the average computing time can be reduced and shorter trajectories in both time and path length are obtained with the proposed approach.

Keywords: singularity avoidance, motion planning, trajectory optimization, manipulability, redundant manipulators

1. INTRODUCTION

Several important tasks in robotics require compliance in the robot's end-effector including handling tasks, such as the peg-in-hole task, see, e.g., Park et al. (2017) and Song et al. (2021), or more recently tasks in physical human-robot interaction (pHRI), see, e.g., Sharifi et al. (2022) and Li et al. (2018). To this end, control concepts enabling compliance in the end-effector, e.g., prescribing a specific impedance as done in Ott (2008), are required. However, such control concepts in Cartesian space rely on the non-singularity of the manipulator Jacobian or of the pseudo-inverse in the redundant case. To ensure that no singularity occurs during control execution, approaches can be divided into two general categories.

In the first category, additional measures are taken in the controller to ensure the invertibility of the Jacobian during execution even at singular reference configurations. This was investigated intensively in the area of numerical inverse kinematics algorithms. Popular approaches include damped least-squares inverse solutions, see, e.g., Chiaverini (1997); Buss and Kim (2005), and singular value filtering, see, e.g., Colomé and Torras (2015). Furthermore, the manipulability measure proposed by Yoshikawa (1985) can be used as a proxy for singularity avoidance. The manipulability measure is proportional to the volume of the manipulability ellipsoid of the manipulator. Therefore, a value larger than zero of this measure implies the non-singularity of the manipulator Jacobian. However, this manipulability measure is not directly a distance measure to singularities since in degenerate cases of the manipulability ellipsoid the volume can be large even if one direction

almost collapses. Manipulability maximization for inverse kinematics is done, e.g., in Dufour and Suleiman (2017). A potential function on the torque level, as an additive impedance, based on the manipulability measure is proposed in Ott (2008) for singularity avoidance. Due to the complexity introduced by maximizing the manipulability measure, an optimization approach using a dynamic neural network is introduced in Jin et al. (2017) for tracking control including the consideration of joint velocity limits.

In the second category, trajectories are planned such that no singularities occur. This has the main advantage that other objectives and constraints can be taken into account during planning. Similar to optimization-based inverse kinematics, these aspects can be included over the whole trajectory horizon and not only locally at every point in the inverse kinematics. Consider for example an obstacle-free trajectory that is executed with a task-space controller implementing one of the singularity avoidance concepts of the first category. Since the controller does not know anything about the obstacles in the environment it may happen that due to singularity avoidance the robot deviates from the planned trajectory and crashes into an obstacle. Furthermore, the controller only reacts instantaneously and is unable to predict a potential crash or a violation of the joint limit. In contrast, if the planned trajectory is obstacle free and singularity free, the trajectory can be executed without violating any of these constraints, assuming the trajectory tracking controller is able to follow the desired trajectory. Closely related to the inverse kinematics approaches, a joint-space trajectory generation algorithm which maximizes manipulability based on a task-space trajectory is presented in Guilamo et al. (2006). This algorithm is classified as a search-based method which

¹ These authors contributed equally to this work.

guarantees resolution completeness and global optimality but is computationally quite complex. Furthermore, it does not solve the full planning problem but relies on a known task-space reference and does not provide any possibility to include further optimization criteria. In Menasri et al. (2013), a path planning approach for manipulability maximization and obstacle avoidance using a bi-level genetic algorithm is proposed. The algorithm is demonstrated in simulation on a robot with 5 degrees of freedom (DoF), but no results with respect to execution time and the real-time capabilities are reported. A fast manipulability maximization for trajectory optimization using Gaussian processes is done in Marić et al. (2019). The authors demonstrate fast singularity avoidance combined with obstacle avoidance in planning. However, general joint-space constraints are not considered, which typically increase the computation time significantly. Another approach presented in Kaden and Thomas (2019), classified as a two-step approach, combines sampling-based planning, i.e., Rapidly Exploring Random Trees (RRTs), see, e.g., LaValle and James (2001), with Gaussian Mixture Models and STOMP, see Kalakrishnan et al. (2011), for trajectory smoothing. Note that in Kaden and Thomas (2019) the state costs take into account the corresponding manipulability. The main advantage of this approach is the capability to escape local minima with sampling-based planning compared to directly optimizing the trajectory. The two-step process, on the other hand, is computationally expensive.

In this work, a novel singularity avoidance concept based on known singularities and potential functions is proposed. The proposed approach is compared to manipulability maximization in terms of trajectory quality in the vicinity of singularities and suitability for online trajectory optimization. For a representative evaluation, three serial manipulators are considered in this work. The 6-DoF industrial COMAU Racer 7-1.4 represents a commonly used industrial robot. As examples of collaborative robots, the non-offset 7-DoF KUKA LBR iiwa R820 and the 7-DoF offset FRANKA EMIKA Panda are investigated. Due to the offset in the kinematics, the singular configurations of the FRANKA EMIKA Panda differ significantly from the KUKA LBR iiwa R820. To the best of the authors' knowledge, the analytic singular configurations of the COMAU Racer 7-1.4 and the FRANKA EMIKA Panda have not been presented in the literature so far.

The paper is organized as follows: In Section 2, the kinematic model of a rigid-body serial manipulator is described and the singular configurations are determined. In addition, the trajectory optimization used in this work is introduced. The novel singularity avoidance approach for trajectory optimization based on potential functions is presented in Section 3. The statistical evaluation of the proposed approach and the manipulability maximization is discussed in Section 4. Finally, Section 5 concludes the paper and gives an outlook on future work.

2. MATHEMATICAL MODEL

In this section, the derivation of the forward kinematics and the manipulator Jacobian of serial manipulators are presented. Furthermore, the dynamics of the rigid-body manipulators are described including a Cartesian inverse dynamics control law. The compensation of the nonlinear

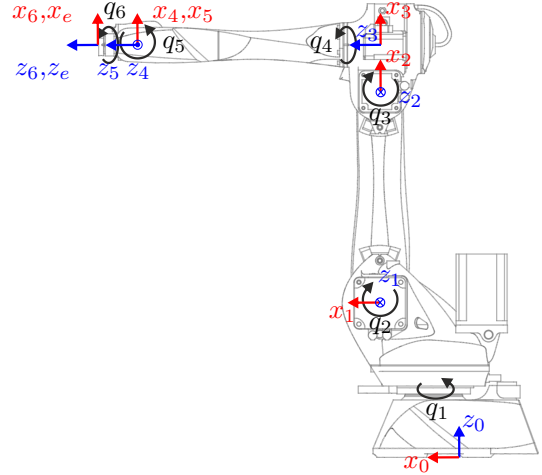


Fig. 1. Schematic of the COMAU Racer 7-1.4.

dynamics justifies the use of a linear model for the presented trajectory optimization approach.

2.1 Forward kinematics

In robotics, the forward kinematics determines the geometric relation between the joint space, i.e., coordinates of the robot joints, and the operational space, i.e., the position in 3D space and the orientation of the robot end-effector. The geometric relation can be systematically computed by using the homogeneous transformation

$$\mathbf{H}_m^n = \begin{bmatrix} \mathbf{R}_n^m & \mathbf{d}_n^m \\ \mathbf{0} & 1 \end{bmatrix}, \quad (1)$$

where the distance vector $\mathbf{d}_n^m \in \mathbb{R}^3$ and the orthogonal rotation matrix $\mathbf{R}_n^m \in SO(3)$ represent the translation of the origin and the rotation from the coordinate frame n to the coordinate frame m , respectively. Pure translations in the direction of the local axis $i \in \{x, y, z\}$ by the length d and pure rotations by the angle φ around the local axis i are denoted by $\mathbf{H}_{T_i,d}$ and $\mathbf{H}_{R_i,\varphi}$, respectively.

Homogeneous transformations of serial robot manipulators are described using successive homogeneous transformations \mathbf{H}_{i-1}^i with the Denavit-Hartenberg (DH) convention, see Spong et al. (2006), consisting of two rotations and two translations in the form

$$\mathbf{H}_{i-1}^i = \mathbf{H}_{R_z,\theta_i} \mathbf{H}_{T_z,d_i} \mathbf{H}_{T_x,a_i} \mathbf{H}_{R_x,\alpha_i}, \quad (2)$$

with the four parameters d_i , θ_i , a_i , and α_i for each joint i . Thus, the forward kinematics of a rigid-body manipulator with M joints is computed in the form

$$\mathbf{H}_0^M = \mathbf{H}_0^1 \mathbf{H}_1^2 \dots \mathbf{H}_{M-1}^M, \quad (3)$$

The COMAU Racer 7-1.4 consists of 6 rotational joints. Its schematics and DH parameters are listed in Fig. 1 and Tab. 1(a), respectively. The KUKA LBR iiwa R820 is a non-offset 7-DoF serial manipulator with all offset parameters a_i equal to zero, see Tab. 1(b) and Fig. 2(a) and the FRANKA EMIKA Panda is an offset 7-DoF serial manipulator with non-zero parameters a_i , see Tab. 1(c) and Fig. 2(b).

Substituting the DH parameters of an M -DoF serial manipulator in Tab. 1 into (3) with the joint coordinates $\mathbf{q}^T = [q_1, q_2, \dots, q_M]$ yields the homogeneous transformation of the Cartesian end-effector pose

$$\mathbf{H}_e(\mathbf{q}) = \mathbf{H}_0^M = \begin{bmatrix} \mathbf{R}_e(\mathbf{q}) & \mathbf{p}_e(\mathbf{q}) \\ \mathbf{0} & 1 \end{bmatrix}, \quad (4)$$

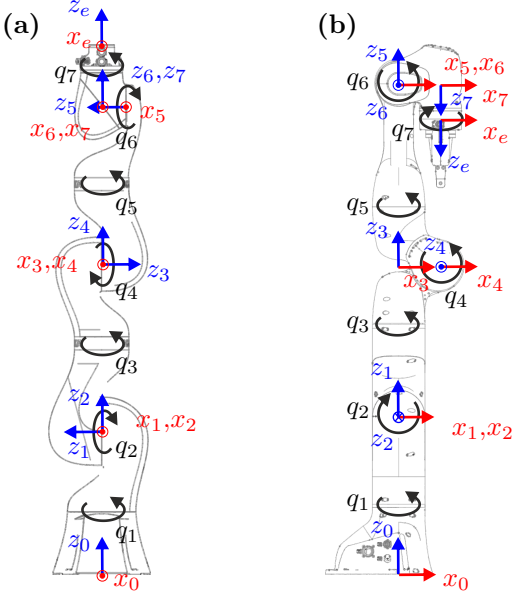


Fig. 2. (a) Schematics of the KUKA LBR iiwa R820 on the left-hand side, and (b) schematics of the FRANKA EMIKA Panda on the right-hand side.

Table 1. Denavit-Hartenberg parameters.

| (a) COMAU Racer 7-1.4 | | | | | | | | | |
|-----------------------|------------|-------|-------|-----------------|-----|------------|-------|-------|------------------|
| i | θ_i | d_i | a_i | α_i | i | θ_i | d_i | a_i | α_i |
| 1 | q_1 | d_1 | a_1 | $\frac{\pi}{2}$ | 4 | q_4 | d_4 | 0 | $-\frac{\pi}{2}$ |
| 2 | q_2 | 0 | a_2 | 0 | 5 | q_5 | 0 | 0 | $\frac{\pi}{2}$ |
| 3 | q_3 | 0 | a_3 | $\frac{\pi}{2}$ | 6 | q_6 | d_6 | 0 | 0 |

| (b) KUKA LBR iiwa R820 | | | | | | | | | |
|------------------------|------------|-------|-------|------------------|-----|------------|-------|-------|------------------|
| i | θ_i | d_i | a_i | α_i | i | θ_i | d_i | a_i | α_i |
| 1 | q_1 | d_1 | 0 | $\frac{\pi}{2}$ | 5 | q_5 | d_5 | 0 | $-\frac{\pi}{2}$ |
| 2 | q_2 | 0 | 0 | $-\frac{\pi}{2}$ | 6 | q_6 | 0 | 0 | $-\frac{\pi}{2}$ |
| 3 | q_3 | d_3 | 0 | $-\frac{\pi}{2}$ | 7 | q_7 | 0 | 0 | 0 |
| 4 | q_4 | 0 | 0 | $\frac{\pi}{2}$ | e | 0 | d_e | 0 | 0 |

| (c) FRANKA EMIKA Panda | | | | | | | | | |
|------------------------|------------|-------|-------|------------------|-----|------------|-------|-------|------------------|
| i | θ_i | d_i | a_i | α_i | i | θ_i | d_i | a_i | α_i |
| 1 | q_1 | d_1 | 0 | 0 | 5 | q_5 | d_5 | a_5 | $-\frac{\pi}{2}$ |
| 2 | q_2 | 0 | 0 | $-\frac{\pi}{2}$ | 6 | q_6 | 0 | 0 | $\frac{\pi}{2}$ |
| 3 | q_3 | d_3 | 0 | $\frac{\pi}{2}$ | 7 | q_7 | 0 | 0 | $\frac{\pi}{2}$ |
| 4 | q_4 | 0 | a_4 | $\frac{\pi}{2}$ | e | 0 | d_e | 0 | 0 |

where \mathbf{p}_e and \mathbf{R}_e are the end-effector position and orientation expressed in the world frame, respectively.

2.2 Manipulator Jacobian

The velocity of the end-effector pose (4) is computed by the geometric manipulator Jacobian $\mathbf{J}_e(\mathbf{q})$ as

$$\begin{bmatrix} \dot{\mathbf{p}}_e \\ \boldsymbol{\omega}_e \end{bmatrix} = \begin{bmatrix} \mathbf{J}_{e,v}(\mathbf{q}) \\ \mathbf{J}_{e,\omega}(\mathbf{q}) \end{bmatrix} \dot{\mathbf{q}} = \mathbf{J}_e(\mathbf{q}) \dot{\mathbf{q}}, \quad (5)$$

with the linear end-effector velocity $\dot{\mathbf{p}}_e$ and the angular end-effector velocity $\boldsymbol{\omega}_e^T = [\omega_x, \omega_y, \omega_z]$. The latter results from the skew-symmetric matrix operator $\mathbf{S}(\boldsymbol{\omega}_e)$ as

$$\mathbf{S}(\boldsymbol{\omega}) = \dot{\mathbf{R}}_e \mathbf{R}_e^T = \begin{bmatrix} 0 & -\omega_z & \omega_y \\ \omega_z & 0 & -\omega_x \\ -\omega_y & \omega_x & 0 \end{bmatrix}. \quad (6)$$

In other words, the geometric manipulator Jacobian $\mathbf{J}_e(\mathbf{q})$ describes the relationship between the joint-space velocity $\dot{\mathbf{q}} \in \mathbb{R}^M$ and the translational and angular velocities in the task space.

2.3 Singularity Analysis

A robot configuration, causing the robot end-effector to lose the ability to move in one or more directions is called a singularity. Using (5), the task-space end-effector velocity $\mathbf{v}_{ts}^T = [\dot{\mathbf{p}}_e^T, \boldsymbol{\omega}_e^T]$ is expressed in the form

$$\begin{aligned} \mathbf{v}_{ts} &= \begin{bmatrix} \dot{\mathbf{p}}_e \\ \boldsymbol{\omega}_e \end{bmatrix} = [\mathbf{J}_{e,c_1} \cdots \mathbf{J}_{e,c_M}] \begin{bmatrix} \dot{q}_1 \\ \vdots \\ \dot{q}_M \end{bmatrix} \\ &= \sum_{i=1}^M \mathbf{J}_{e,c_i} \dot{q}_i, \end{aligned} \quad (7)$$

where \mathbf{J}_{e,c_i} is the i -th column of the Jacobian $\mathbf{J}_e(\mathbf{q})$. Hence, the geometric manipulator Jacobian $\mathbf{J}_e(\mathbf{q})$ can be utilized to identify singular configurations. A robot configuration \mathbf{q} is singular if

$$\text{Rank}(\mathbf{J}_e(\mathbf{q})) < 6, \quad (8)$$

or, similarly,

$$m(\mathbf{q}) = \sqrt{\det(\mathbf{J}_e \mathbf{J}_e^T)} = 0, \quad (9)$$

which is called singularity index $m(\mathbf{q})$, see Yoshikawa (1985). Note that the mathematical definition of a kinematic singularity, e.g., (8), is independent of the choice of the reference frame of the end-effector Jacobian $\mathbf{J}_e(\mathbf{q})$, see, Lynch and Park (2017). To reduce the complexity of the expression of $\mathbf{J}_e(\mathbf{q})$ in the world frame, the manipulator Jacobian is transformed into the end-effector frame

$$\mathbf{J}_e^M(\mathbf{q}) = \begin{bmatrix} \mathbf{R}_e^T & \mathbf{0} \\ \mathbf{0} & \mathbf{R}_e^T \end{bmatrix} \mathbf{J}_e(\mathbf{q}), \quad (10)$$

for the singularity analysis.

In the following, the general scheme for singularity analysis of the COMAU Racer 7-1.4 is presented. Based on this scheme, the singularity analysis of the KUKA LBR iiwa R820 and the FRANKA EMIKA Panda are briefly summarized. The symbolic expression of the manipulator Jacobian of the 6-DoF COMAU Racer 7-1.4 in its end-effector frame is of the form

$$\mathbf{J}_e^6(\mathbf{q}) = \begin{bmatrix} \mathbf{J}_{e,r_1}^6 \\ \vdots \\ \mathbf{J}_{e,r_6}^6 \end{bmatrix} = \begin{array}{c|ccc} & 0 & d_6 & 0 \\ \mathbf{J}_{e,11}^6 & \sin(q_5)d_6 & 0 & 0 \\ & 0 & 0 & 0 \\ \hline \mathbf{J}_{e,21}^6 & -\sin(q_5) & 0 & 0 \\ & 0 & 1 & 0 \\ & \cos(q_5) & 0 & 1 \end{array}, \quad (11)$$

where \mathbf{J}_{e,r_i}^6 is the i -th row of $\mathbf{J}_e^6(\mathbf{q})$, $\mathbf{J}_{e,11}^6 \in \mathbb{R}^{3 \times 3}$, $\mathbf{J}_{e,21}^6 \in \mathbb{R}^{3 \times 3}$ and

$$\mathbf{J}_{e,22}^6 = \begin{bmatrix} -\sin(q_5) & 0 & 0 \\ 0 & 1 & 0 \\ \cos(q_5) & 0 & 1 \end{bmatrix}, \quad (12)$$

are submatrices of $\mathbf{J}_e^6(\mathbf{q})$. Applying the following row operations, see, e.g., Xu et al. (2015),

$$\begin{aligned} \text{(A)} & \mathbf{J}_{e,r_1} - d_6 \mathbf{J}_{e,r_5} \rightarrow \mathbf{J}_{e,r_1} \\ \text{(B)} & \mathbf{J}_{e,r_2} + d_6 \mathbf{J}_{e,r_4} \rightarrow \mathbf{J}_{e,r_2} \end{aligned}$$

to \mathbf{J}_e^6 from (11) results in

$$\mathbf{J}_e^{6t} = \begin{array}{c|ccc} & 0 & 0 & 0 \\ \mathbf{J}_{e,11}^{6t} & 0 & 0 & 0 \\ & 0 & 0 & 0 \\ \hline \mathbf{J}_{e,21}^6 & \mathbf{J}_{e,22}^6 & & \end{array}. \quad (13)$$

Note that the rank of a matrix remains invariant under elementary row operations. Since $\mathbf{J}_{e,11}^{6t}$ and $\mathbf{J}_{e,22}^{6t}$ have to be full rank for \mathbf{J}_e^6 to be non-singular, the determinants of $\mathbf{J}_{e,11}^{6t}$ and $\mathbf{J}_{e,22}^{6t}$ are computed to identify the singular configurations

$$(A) \quad q_5 = 0 \quad (14a)$$

$$(B) \quad q_3 = \arctan\left(\frac{d_4}{a_3}\right) \quad (14b)$$

$$(C) \quad a_1 + \cos(q_2)a_2 + a_3 \cos(q_2 + q_3) + d_4 \sin(q_2 + q_3) = 0. \quad (14c)$$

In a similar way, the singularity analysis of a 7-DoF serial manipulator is performed by applying row operations of the corresponding manipulator Jacobian in the end-effector coordinate \mathbf{J}_e^7 . This leads to the transformed manipulator Jacobian \mathbf{J}_e^{7t} consisting of four submatrices in the form

$$\mathbf{J}_e^{7t} = \left[\begin{array}{c|ccc} \mathbf{J}_{e,11}^{7t} & 0 & 0 & 0 \\ \hline & 0 & 0 & 0 \\ & 0 & 0 & 0 \\ \hline \mathbf{J}_{e,21}^{7t} & & \mathbf{J}_{e,22}^{7t} & \end{array} \right], \quad (15)$$

where $\mathbf{J}_{e,11}^{7t} \in \mathbb{R}^{3 \times 4}$ and $\mathbf{J}_{e,22}^{7t} \in \mathbb{R}^{3 \times 3}$. Here, similar to (13), the two submatrices $\mathbf{J}_{e,11}^{7t}$ and $\mathbf{J}_{e,22}^{7t}$ must have full rank. Since $\mathbf{J}_{e,11}^{7t} \in \mathbb{R}^{3 \times 4}$ is a non-square matrix, the determinant

$$\det(\mathbf{J}_{e,11}^{7t} (\mathbf{J}_{e,11}^{7t})^T) \quad (16)$$

is checked instead. To reduce the computational complexity of (16), the Cauchy-Binet theorem is used, see, e.g., Knill (2014). This allows to express (16) as a sum of squares in the form

$$\det(\mathbf{J}_{e,11}^{7t} (\mathbf{J}_{e,11}^{7t})^T) = \sum_{s \in S} [\det(\mathbf{J}_{e,11,s}^{7t})]^2, \quad (17)$$

where S is the set of 3-combinations of $\{1, \dots, 4\}$ and $\mathbf{J}_{e,11,s}^{7t} \in \mathbb{R}^{3 \times 3}$ is formed by columns of $\mathbf{J}_{e,11}^{7t}$ at indices from the subset s . Note that a 3-combination of $\{1, \dots, 4\}$ is a subset of three distinct elements of the set $\{1, \dots, 4\}$, see Roberts and Tesman (2009). Thereby, singular configurations can be identified by analyzing the determinants of $\mathbf{J}_{e,11,s}^{7t}$, which is much simpler than considering (16). Due to the limited length of the paper, the detailed analysis of (17) for the KUKA LBR iiwa R820 and the FRANKA EMIKA Panda is omitted here and all singular configurations for these 7-DoF robots are listed in the Appendix.

2.4 Dynamics

The dynamical rigid-body model of a serial manipulator is given by

$$\mathbf{M}(\mathbf{q})\ddot{\mathbf{q}} + \mathbf{C}(\mathbf{q}, \dot{\mathbf{q}})\dot{\mathbf{q}} + \mathbf{g}(\mathbf{q}) = \boldsymbol{\tau}, \quad (18)$$

with the positive definite inertia matrix $\mathbf{M}(\mathbf{q})$, the Coriolis matrix $\mathbf{C}(\mathbf{q}, \dot{\mathbf{q}})$ and the vector of gravitational forces $\mathbf{g}(\mathbf{q})$. The generalized torques are denoted by $\boldsymbol{\tau}$. It is assumed that the nonlinear dynamics are compensated by an inverse dynamics control law of the form

$$\boldsymbol{\tau} = \mathbf{M}(\mathbf{q})\mathbf{v} + \mathbf{C}(\mathbf{q}, \dot{\mathbf{q}})\dot{\mathbf{q}} + \mathbf{g}(\mathbf{q}), \quad (19)$$

resulting in the remaining linear dynamics

$$\ddot{\mathbf{q}} = \mathbf{v}, \quad (20)$$

with the virtual input \mathbf{v} . Different approaches exist for stabilizing the linear system including Cartesian impedance

control. In the following, a reference trajectory is planned for this remaining linear dynamics.

2.5 Trajectory Optimization

The trajectory optimization problem is formulated in the joint space. If Cartesian reference trajectories are required, they can be uniquely calculated using the forward kinematics and differential kinematics of the manipulator. The trajectory optimization is implemented using a direct transcription method, discretizing the trajectory into N grid points and solving the discrete optimization problem

$$\min_{\boldsymbol{\xi}} t_F + \sum_{k=0}^{N-1} [\mathbf{v}_k^T \mathbf{v}_k + L_{\text{sing}}(\mathbf{q}_k)] \quad (21a)$$

$$\text{s.t.} \quad \mathbf{x}_{k+1} = \boldsymbol{\Phi} \mathbf{x}_k + \boldsymbol{\Gamma} \mathbf{v}_k \quad (21b)$$

$$\mathbf{x}_0 = \mathbf{x}_S, \quad \mathbf{x}_{N-1} = \mathbf{x}_T \quad (21c)$$

$$\underline{\mathbf{x}} \leq \mathbf{x}_k \leq \bar{\mathbf{x}}, \quad k = 0, \dots, N-1 \quad (21d)$$

$$\underline{\mathbf{v}} \leq \mathbf{v}_k \leq \bar{\mathbf{v}}, \quad k = 0, \dots, N-1 \quad (21e)$$

$$t_F \geq 0 \quad (21f)$$

with the state $\mathbf{x}_k^T = [\mathbf{q}_k^T, \dot{\mathbf{q}}_k^T]$, the input \mathbf{v}_k , and

$$\boldsymbol{\xi}^T = [t_F, \mathbf{x}_0, \dots, \mathbf{x}_{N-1}, \mathbf{v}_0, \dots, \mathbf{v}_{N-1}].$$

The constraints (21c) describe the start- and the end-point constraints. The constraints on the optimization variables are given in (21d), (21e), and (21f). The discretized dynamics of the double integrator system (20) with the sampling time $h = t_F/N$ reads as

$$\boldsymbol{\Phi} = \begin{bmatrix} 1 & h \\ 0 & 1 \end{bmatrix} \otimes \mathbf{I}_M \quad (22a)$$

$$\boldsymbol{\Gamma} = \begin{bmatrix} h^2 \\ 2h \end{bmatrix} \otimes \mathbf{I}_M. \quad (22b)$$

The operator \otimes describes the Kronecker product and \mathbf{I}_M is the identity matrix of size M . The objective function consists of minimizing the time t_F , a regularization term $\mathbf{v}_k^T \mathbf{v}_k$, and a singularity avoidance term $L_{\text{sing}}(\mathbf{q}_k)$. The objective functions for singularity avoidance considered in this paper are discussed in the following section.

3. SINGULARITY AVOIDANCE

This section presents two objective function formulations for singularity avoidance. First, an approach for directly maximizing the manipulability known from the literature is discussed. Second, a novel approach formulating the singularity avoidance using potential functions for known singularities based on the calculations in Section 2.3 is presented.

Strict singularity avoidance can be achieved by constraining the kinematic manipulability measure (9) to stay above a certain minimum value, as done, e.g., in Marani et al. (2002). For fast online planning, however, a formulation based on an objective function is often preferable and leads to a faster convergence of the optimization. To maximize manipulability, the objective function can be formulated as

$$L_{\text{sing},1}(\mathbf{q}) = \frac{w_m}{m(\mathbf{q}) + \varepsilon}. \quad (23)$$

The parameter $\varepsilon > 0$ ensures that the expression remains well defined even for $m(\mathbf{q}) = 0$ and $w_m > 0$ is a weighting parameter. Note that this does not strictly avoid singularities in all cases but leads to good results in practise provided that the weight w_m is chosen large enough compared

to the other terms in the objective function. The main disadvantage of this formulation is that the evaluation of $m(\mathbf{q})$, see, e.g., (33) and (34), is computationally expensive especially for the gradients required for the optimization algorithm. Hence, this approach is not suitable for fast optimization-based planning. In addition, since the manipulability measure is related only to the volume of the manipulability ellipsoid, it does not necessarily indicate a short distance to a singularity.

To this end, a different approach based on potential functions is proposed, where the objective function is increased close to singular configurations of the manipulator. Common structures of serial manipulators allow the calculation of those singular configurations analytically via the manipulator Jacobian (8) in form of explicit or implicit equations, see, e.g., (14) or (36). These equations are less complex compared to the manipulability measure (9). From this calculation, implicit functions of the form $\psi(\mathbf{q}) = 0$ can be obtained that are exactly zero if the manipulator Jacobian is singular.

For example, the singularities of the KUKA LBR iiwa R820 are caused by one or two joints, see (35). Hence, for a single-joint singularity condition, the i -th equation reads as

$$\psi_i(q_m) = (q_m - q_{m,s})^2 \quad (24)$$

for a singularity at $q_{m,s}$ and

$$\psi_i(q_m, q_n) = (q_m - q_{m,s})^2 + (q_n - q_{n,s})^2 \quad (25)$$

for a singularity caused by two joints q_m and q_n at $q_{m,s}$ and $q_{n,s}$ simultaneously. Given a general function $\psi_i(\mathbf{q})$, the potential function for a singularity is then introduced in the form

$$\varphi_i(\mathbf{q}) = \exp(\eta_{1,i} - \eta_{2,i}\psi_i(\mathbf{q})) . \quad (26)$$

Note that the parameters $\eta_{1,i} > 0$ and $\eta_{2,i} > 0$ define the peak value and the width of the potential function, respectively.

The overall cost function for singularity avoidance $L_{\text{sing},2}(\mathbf{q})$ is then given by

$$L_{\text{sing},2}(\mathbf{q}) = w_m \sum_i \varphi_i(\mathbf{q}) . \quad (27)$$

The gradient and Hessian of (27) can be easily calculated and the computational costs are significantly smaller compared to (9). Another advantage of this approach is that (24) and (25) are joint-space distance measures directly for the singularities instead of the volume proxy utilized in the singularity index (9).

4. RESULTS

In this section, the proposed singularity avoidance concept for online trajectory optimization is evaluated in comparison to the direct manipulability maximization.

For this, Monte Carlo simulations are performed with the three robots from Section 2. For each robot, $N_{\text{mc}} = 10^4$ pairs of initial robot configurations $\mathbf{x}_S^T = [\mathbf{q}_0^T, \mathbf{0}^T]$ and target configurations $\mathbf{x}_T^T = [\mathbf{q}_T^T, \mathbf{0}^T]$ are randomly selected in the workspace from a uniform distribution in the admissible ranges. In addition, configurations with a manipulability of less than 1×10^{-4} are excluded. The trajectory optimization (21) is evaluated for three different objectives, i.e. without singularity avoidance, with the

manipulability-based objective (23), and with the proposed singularity avoidance approach (27). The interior-point solver IPOPT, see Wächter and Biegler (2006), with the linear solver MA27, see Duff (2004), is employed to solve the optimization problem (21). Additionally, the gradient and the Hessian are computed using CasADi, see Andersson et al. (2019). The trajectory optimization in (21) is discretized with $N = 30$ collocation points giving a total of 631 optimization variables for the 7 DoF and 541 for the 6 DoF manipulator.

To compare the performance of the three objective functions, the following indices are computed and are evaluated statistically.

- The minimum value of the manipulability measure (9) over all Monte Carlo samples

$$m_{\min} = \min m(\mathbf{q}_{k,i}) , \quad (28)$$

$$k = 0, \dots, N-1, \quad i = 1, \dots, N_{\text{mc}} .$$

- The maximum value of the manipulability measure (9) over all Monte Carlo samples

$$m_{\max} = \max m(\mathbf{q}_{k,i}) , \quad (29)$$

$$k = 0, \dots, N-1, \quad i = 1, \dots, N_{\text{mc}} .$$

- The average value of the manipulability measure (9) for each Monte Carlo sample $i = 1, \dots, N_{\text{mc}}$

$$m_{\text{avg},i} = \frac{1}{N} \sum_{k=0}^{N-1} m(\mathbf{q}_{k,i}) . \quad (30)$$

- The approximate length of the 3D end-effector path for each Monte Carlo sample $i = 1, \dots, N_{\text{mc}}$

$$l_{\text{p},i} = \sum_{k=1}^{N-1} \sqrt{\Delta_{k,i}^T \Delta_{k,i}} , \quad (31)$$

with $\Delta_{k,i} = \mathbf{p}_e(\mathbf{q}_{k,i}) - \mathbf{p}_e(\mathbf{q}_{k-1,i})$. The function $\mathbf{p}_e(\mathbf{q})$ computes the position of the end-effector in 3D, as defined in (4).

- The sum of differences in rotation, see, e.g., Huynh (2009), along the 3D path for each Monte Carlo sample $i = 1, \dots, N_{\text{mc}}$

$$l_{\text{quat},i} = \sum_{k=1}^{N-1} \delta_{k,i} , \quad (32)$$

with $\delta_{k,i} = 1 - \text{quat}(\mathbf{R}_e(\mathbf{q}_{k,i}))^T \text{quat}(\mathbf{R}_e(\mathbf{q}_{k-1,i}))$. The function $\text{quat}(\mathbf{R})$ transforms a rotation matrix \mathbf{R} into its corresponding quaternion, see, e.g., Shepperd (1978).

The results of the Monte Carlo simulation are summarized in Tab. 2, Tab. 3, and Tab. 4 for the COMAU Racer 7-1.4, the KUKA LBR iiwa R820 and the FRANKA EMIKA Panda, respectively. For the trajectory duration t_F , the computation time, the average manipulability of a single trajectory (30), the approximate path length (31) and the change in orientation (32), the mean and the standard deviation over all Monte Carlo samples are reported. It can be observed that both singularity avoidance schemes increase the average trajectory duration compared to the baseline without singularity avoidance. This is not surprising because avoiding a singularity typically leads to a deviation from the shortest path. The proposed singularity

Table 2. COMAU Racer 7-1.4

Performance evaluation of the proposed singularity avoidance (SA) for trajectory optimization in comparison to manipulability maximization.

| | without SA | Max. SA | Proposed SA |
|-------------------|-------------------|------------------|-----------------|
| t_F (s) | 2.3174 ± 0.46 | 3.82 ± 0.73 | 4.07 ± 2.15 |
| comp. time (ms) | 10.4 ± 5.8 | 27.3 ± 18.3 | 21.5 ± 15.8 |
| m_{\min} | 2.01^{-7} | 6.6^{-6} | 1.01^{-4} |
| m_{\max} | 0.466 | 0.466 | 0.466 |
| m_{avg} | 0.16 ± 0.08 | 0.362 ± 0.04 | 0.19 ± 0.07 |
| l_p | 2.42 ± 1.35 | 4.03 ± 1.6 | 3.86 ± 2.36 |
| l_{quat} | 1.52 ± 1.35 | 2.2 ± 1.65 | 1.92 ± 1.46 |

Table 3. KUKA LBR iiwa R820

Performance evaluation of the proposed singularity avoidance (SA) for trajectory optimization in comparison to manipulability maximization.

| | without SA | Max. SA | Proposed SA |
|-------------------|-------------------|------------------|------------------|
| t_F (s) | 2.67 ± 0.49 | 9.83 ± 1.83 | 7.01 ± 2.94 |
| comp. time (ms) | 10.9 ± 5 | 61.5 ± 27.9 | 56.6 ± 35 |
| m_{\min} | 5.6^{-8} | 1.82^{-07} | 1.03^{-4} |
| m_{\max} | 0.15 | 0.16 | 0.159 |
| m_{avg} | 0.055 ± 0.025 | 0.14 ± 0.004 | 0.07 ± 0.023 |
| l_p | 2.1 ± 0.92 | 3.58 ± 1.15 | 2.53 ± 0.96 |
| l_{quat} | 1.67 ± 1.45 | 3.54 ± 2.19 | 2.19 ± 1.78 |

avoidance scheme, however, leads to a shorter duration of the trajectories on average compared to the manipulability maximization, except for the COMAU Racer 7-1.4 which could be possible because less alternative trajectories are available for a non-redundant manipulator. This can also be seen in the average path length measures (31) and (32) being the longest for the manipulability maximization approach, also for the COMAU Racer 7-1.4. The reason is that the proposed approach only influences the trajectories locally around possible singularities and not globally along the entire trajectory. In contrast, due to this global influence of the manipulability, the manipulability maximization approach leads to higher manipulability on average (30) along the whole trajectories. Hence, if maximization of the manipulability is desired instead of singularity avoidance, considering it directly is the better approach. On the other hand, the minimum value of the manipulability according to (28) is larger for the proposed approach, which also shows the superiority in terms of singularity avoidance. In practice, the achieved minimum manipulability depends on the weighting of the objective terms and must be chosen carefully to avoid large control torques. Since the workspace of the manipulators is well covered by the Monte Carlo sampling, the maximum manipulability (29) achieved is very similar with both approaches. One of the main advantages of the proposed approach is the reduced average computation time making it more suitable for online trajectory optimization. For simpler kinematics, like the KUKA LBR iiwa R820 or the COMAU Racer 7-1.4, the difference is only a few milliseconds, but for the FRANKA EMIKA Panda with a significantly larger expression for the manipulability, this advantage is much more pronounced.

Table 4. FRANKA EMIKA Panda

Performance evaluation of the proposed singularity avoidance (SA) for trajectory optimization in comparison to manipulability maximization.

| | without SA | Max. SA | Proposed SA |
|-------------------|-----------------|-------------------|--------------------|
| t_F (s) | 2.44 ± 0.29 | 11.3 ± 2.29 | 4.96 ± 3.11 |
| comp. time (ms) | 11.1 ± 5.5 | 245.3 ± 377 | 72.3 ± 57.5 |
| m_{\min} | 6.5^{-6} | 6.82^{-5} | 3.07^{-4} |
| m_{\max} | 0.128 | 0.13 | 0.129 |
| m_{avg} | 0.04 ± 0.02 | 0.112 ± 0.012 | 0.057 ± 0.0188 |
| l_p | 1.34 ± 0.69 | 2.37 ± 0.81 | 1.866 ± 0.953 |
| l_{quat} | 1.76 ± 1.46 | 3.62 ± 2.13 | 2.41 ± 1.81 |

5. CONCLUSION

In this work, an approach for singularity avoidance based on potential functions around known singular configurations for online trajectory optimization of serial manipulators is presented. Singular configurations were calculated for three different robots, the COMAU Racer 7-1.4, the KUKA LBR iiwa R820, and the FRANKA EMIKA Panda. The proposed approach is compared to the well-known manipulability maximization in a Monte Carlo simulation. The results show that the proposed approach speeds up the singularity avoidance in online trajectory optimization in all of the investigated cases. The advantage becomes more significant for more complex kinematic structures. On the other hand, the proposed approach is not a full replacement for manipulability maximization if high average manipulability is required. Another benefit of the proposed approach is that shorter paths and trajectories with a shorter duration are obtained.

Future work aims at integrating the proposed singularity avoidance approach in real-time trajectory optimization for human-robot interaction applications in combination with Cartesian compliance control. Furthermore, investigating the qualitative properties of the generated trajectories with respect to their path shape is also an interesting point.

APPENDIX

In the following, the abbreviations $s(\cdot) = \sin(\cdot)$ and $c(\cdot) = \cos(\cdot)$ are used for a compact notation.

COMAU Racer 7-1.4:

The square of the manipulability (9) of the COMAU Racer 7-1.4 reads as

$$m^2(\mathbf{q}) = \frac{1}{y^2} a_2^2 s^2(q_5) (a_3 x - d_4)^2 \left[(-2c(q_2)a_2 + a_1) \right. \\ \left. ((-x d_4 - a_3)c(q_2) + s(q_2)(a_3 x - d_4))\sqrt{y} + \right. \\ \left. ((a_2^2 - a_3^2 + d_4^2)x^2 + 4a_3 d_4 x + a_2^2 + a_3^2 - d_4^2)c^2(q_2) + \right. \\ \left. (-2(x d_4 + a_3)(a_3 x - d_4)s(q_2) + 2a_1 a_2 y)c(q_2) + \right. \\ \left. (a_1^2 + a_3^2)x^2 - 2a_3 d_4 x + a_1^2 + d_4^2 \right],$$

with $x = \tan(q_3)$ and $y = x^2 + 1$.

KUKA LBR iiwa R820:

The square of the singularity index (9) of the KUKA LBR iiwa R820 reads as

$$\begin{aligned}
m^2(\mathbf{q}) = & 2d_{se}^2 d_{ew}^2 s^2(q_4) \\
& \left[d_{se}^2 s^2(q_2) s^2(q_4) c^2(q_5) c^2(q_6) + \right. \\
& d_{ew}^2 c^2(q_2) c^2(q_3) s^2(q_4) s^2(q_6) + \\
& (d_{se}^2 + 2d_{se}d_{ew}c(q_4) - d_{ew}^2) s^2(q_2) s^2(q_6) + \\
& \left. \frac{1}{2} (d_{se}^2 c(q_4) + d_{se}d_{ew}) s^2(q_2) s(q_4) c(q_5) s(2q_6) + \right. \\
& \left. \frac{1}{2} (d_{ew}^2 c(q_4) + d_{se}d_{ew}) s(2q_2) c(q_3) s(q_4) s^2(q_6) \right], \tag{34}
\end{aligned}$$

with $d_{se} = d_2 + d_3$ and $d_{ew} = d_4 + d_5$. The singular configurations of the KUKA LBR iiwa R820 are given by

$$(A) \quad q_4 = 0, \tag{35a}$$

$$(B) \quad q_2 = 0 \wedge \left(q_3 = \frac{\pi}{2} \vee q_3 = -\frac{\pi}{2} \right), \tag{35b}$$

$$(C) \quad q_2 = 0 \wedge q_6 = 0, \tag{35c}$$

$$(D) \quad \left(q_5 = \frac{\pi}{2} \vee q_5 = -\frac{\pi}{2} \right) \wedge q_6 = 0, \tag{35d}$$

$$(E) \quad q_4 = \frac{\pi}{2} \wedge q_6 = 0. \tag{35e}$$

FRANKA EMIKA Panda:

Due to the limited length of the paper, the symbolic expression of the singularity index (9) of the FRANKA EMIKA Panda is omitted. However, the source file is provided upon request. The singular configurations of the FRANKA EMIKA Panda are

$$(A) \quad s(q_2) = 0 \wedge c(q_3) = 0 \wedge c(q_5) = 0, \tag{36a}$$

$$(B) \quad c(q_5) = 0 \wedge f_{\text{sing},1}(q_4, q_6) = 0, \tag{36b}$$

$$(C) \quad q_4 = \arctan \left[\frac{a_5(d_3 + d_5)}{-a_5^2 + d_5d_3} \right] \wedge s(q_5) = 0, \tag{36c}$$

$$(D) \quad s(q_2) = 0 \wedge f_{\text{sing},2}(q_3, q_4, q_5, q_6) = 0, \tag{36d}$$

with

$$\begin{aligned}
f_{\text{sing},1}(q_4, q_6) = & c(q_4)a_5[a_7 + (d_3 + d_5)s(q_6)] + \\
& s(q_4)[-a_7d_3 + (a_5^2 - d_5d_3)s(q_6)], \tag{37a}
\end{aligned}$$

$$\begin{aligned}
f_{\text{sing},2}(q_3, q_4, q_5, q_6) = & -a_5(x^2a_5 + yxd_3 + (1-y)a_5) \cdot \\
& c(q_3)a_7c^2(q_5) + a_5s(q_3)(x^2a_5 + yxd_3 + (1-y)a_5) \cdot \\
& a_7s(q_5)c(q_5) - [s(q_6)((a_5^2 - d_5d_3)x + (d_3 + d_5)a_5) - \\
& a_7(d_3x - a_5)]c(q_3)(ya_5 + d_5x - a_5), \tag{37b}
\end{aligned}$$

and $x = \tan(q_4)$ and $y = \sqrt{x^2 + 1}$.

REFERENCES

- Andersson, J.A.E., Gillis, J., Horn, G., Rawlings, J.B., and Diehl, M. (2019). CasADi – A software framework for nonlinear optimization and optimal control. *Mathematical Programming Computation*, 11, 1–36.
- Buss, S.R. and Kim, J.S. (2005). Selectively damped least squares for inverse kinematics. *Journal of Graphics Tools*, 10(3), 37–49.
- Chiaverini, S. (1997). Singularity-robust task-priority redundancy resolution for real-time kinematic control of robot manipulators. *IEEE Transactions on Robotics and Automation*, 13(3), 398–410.
- Colomé, A. and Torras, C. (2015). Closed-loop inverse kinematics for redundant robots: Comparative assessment and two enhancements. *IEEE Transactions on Mechatronics*, 20(2), 944–955.
- Duff, I.S. (2004). MA57: A Code for the Solution of Sparse Symmetric Definite and Indefinite Systems. *ACM Transactions on Mathematical Software*, 30(2), 118–144.
- Dufour, K. and Suleiman, W. (2017). On integrating manipulability index into inverse kinematics solver. In *Proceedings of the International Conference on Intelligent Robots and Systems*, 6967–6972.
- Guilamo, L., Kuffner, J., Nishiwaki, K., and Kagami, S. (2006). Manipulability optimization for trajectory generation. In *Proceedings of the International Conference on Robotics and Automation*, 2017–2022.
- Huynh, D.Q. (2009). Metrics for 3D rotations: Comparison and analysis. *Journal of Mathematical Imaging and Vision*, 35(2), 155–164.
- Jin, L., Li, S., La, H.M., and Luo, X. (2017). Manipulability optimization of redundant manipulators using dynamic neural networks. *IEEE Transactions on Industrial Electronics*, 64(6), 4710–4720.
- Kaden, S. and Thomas, U. (2019). Maximizing robot manipulability along paths in collision-free motion planning. In *Proceedings of the International Conference on Advanced Robotics*, 105–110.
- Kalakrishnan, M., Chitta, S., Theodorou, E., Pastor, P., and Schaal, S. (2011). STOMP: Stochastic trajectory optimization for motion planning. In *Proceedings of the International Conference on Robotics and Automation*, 4569–4574.
- Knill, O. (2014). Cauchy–binet for pseudo-determinants. *Linear Algebra and its Applications*, 459, 522–547.
- LaValle, S. and James, K. (2001). Rapidly-exploring random trees: Progress and prospects. In *Algorithmic and Computational Robotics: New Directions*. CRC Press, New York, USA.
- Li, H.Y., Paranawithana, I., Yang, L., Lim, T.S.K., Foong, S., Ng, F.C., and Tan, U.X. (2018). Stable and compliant motion of physical human–robot interaction coupled with a moving environment using variable admittance and adaptive control. *IEEE Robotics and Automation Letters*, 3(3), 2493–2500.
- Lynch, K.M. and Park, F.C. (2017). *Modern robotics*. Cambridge University Press, Cambridge, United Kingdom.
- Marani, G., Kim, J., Yuh, J., and Chung, W.K. (2002). A real-time approach for singularity avoidance in resolved motion rate control of robotic manipulators. In *Proceedings of the International Conference on Robotics and Automation*, 1973–1978.
- Marić, F., Limoyo, O., Petrović, L., Ablett, T., Petrović, I., and Kelly, J. (2019). Fast manipulability maximization using continuous-time trajectory optimization. In *Proceedings of the International Conference on Intelligent Robots and Systems*, 8258–8264.
- Menasri, R., Nakib, A., Oulhadj, H., Daachi, B., Siarry, P., and Hains, G. (2013). Path planning for redundant manipulators using metaheuristic for bilevel optimization and maximum of manipulability. In *Proceedings of the International Conference on Robotics and Biomimetics*, 145–150.
- Ott, C. (2008). *Cartesian Impedance Control of Redundant and Flexible-Joint Robots*. Springer, Berlin, Heidelberg, Germany.
- Park, H., Park, J., Lee, D.H., Park, J.H., Baeg, M.H., and Bae, J.H. (2017). Compliance-based robotic peg-

- in-hole assembly strategy without force feedback. *IEEE Transactions on Industrial Electronics*, 64(8), 6299–6309.
- Roberts, F. and Tesman, B. (2009). *Applied combinatorics*. CRC Press, Newyork, USA.
- Sharifi, M., Zakerimanesh, A., Mehr, J.K., Torabi, A., Mushahwar, V.K., and Tavakoli, M. (2022). Impedance variation and learning strategies in human–robot interaction. *IEEE Transactions on Cybernetics*, 52(7), 6462–6475.
- Shepperd, S.W. (1978). Quaternion from rotation matrix. *Journal of guidance and control*, 1(3), 223–224.
- Song, J., Chen, Q., and Li, Z. (2021). A peg-in-hole robot assembly system based on gauss mixture model. *Robotics and Computer-Integrated Manufacturing*, 67, 101996.
- Spong, M.W., Hutchinson, S., and Vidyasagar, M. (2006). *Robot modeling and control*, volume 3. Wiley New York, USA.
- Wächter, A. and Biegler, L.T. (2006). On the implementation of an interior-point filter line-search algorithm for large-scale nonlinear programming. *Mathematical Programming*, 106, 25–57.
- Xu, W., Zhang, J., Liang, B., and Li, B. (2015). Singularity analysis and avoidance for robot manipulators with nonspherical wrists. *IEEE Transactions on Industrial Electronics*, 63(1), 277–290.
- Yoshikawa, T. (1985). Manipulability and redundancy control of robotic mechanisms. In *Proceedings of the IEEE International Conference on Robotics and Automation*, 1004–1009.